Compton scattering study of strong orbital delocalization in a LiNiO$_2$ cathode

Veenavee Nipunika Kothalawala [1,*] Kosuke Suzuki,[2] Johannes Nokelainen,[3] Arttu Hyvönen [4] Ilja Makkonen [4]
Bernardo Barbiellini [1,3] Hasnain Hafiz,[3] Pekka Tynjälä,[5,6] Petteri Laine,[5,6] Juho Välikangas [5,6] Tao Hu [5] Ulla Lassi [5,6]
Kodai Takano,[2] Naruki Tsuji,[7] Yosuke Amada,[2] Assa Aravindh Sasikala Devi [8] Matti Alatalo,[8]
Yoshiharu Sakurai [7] Hiroshi Sakurai [2] and Arun Bansil[3]

[1]*Department of Physics, School of Engineering Science, LUT University, FI-53851 Lappeenranta, Finland*
[2]*Graduate School of Science and Technology, Gunma University, Kiryu, Gunma 376-8515, Japan*
[3]*Department of Physics, Northeastern University, Boston, Massachusetts 02115, USA*
[4]*Department of Physics, University of Helsinki, P.O. Box 43, FI-00014 Helsinki, Finland*
[5]*Research Unit of Sustainable Chemistry, University of Oulu, Oulu, Finland*
[6]*Kokkola University Consortium Chydenius, University of Jyvaskyla, Kokkola, Finland*
[7]*Japan Synchrotron Radiation Research Institute (JASRI), Sayo, Hyogo 679-5198, Japan*
[8]*Research Unit of Sustainable Chemistry and Materials and Mechanical Engineering, University of Oulu,
Pentti Kaiteran Katu 1, FI-90570 Oulu, Finland*

Cobalt is used in Li-ion batteries, but it is expensive and could be replaced by nickel to deliver better performance at a lower cost. With this motivation, we discuss how the character of redox orbitals of LiNiO$_2$ can be ascertained through x-ray Compton scattering measurements combined with parallel first-principles simulations. Our analysis reveals the nature of hole states in Li-doped NiO resulting from the hybridization of O $2p$ and Ni $3d$ orbitals. Our study also gives insight into the ferromagnetic ground state and provides a pathway toward the rational design of next-generation battery materials.

I. INTRODUCTION

Compton scattering with hard x rays has proven to be an effective probe of redox processes in battery materials [1,2]. This bulk-sensitive spectroscopy is less sensitive to defects and surfaces compared to the related positron annihilation technique [3]. Both methods, however, provide unique windows into the nature of the redox orbitals and how their subtle characteristics, such as their localization/delocalization properties, evolve during the lithiation and delithiation processes.

The first Compton scattering study in cathode materials by Suzuki *et al.* [4] examined the Li$_x$Mn$_2$O$_4$ (LMO) cathode and showed that the change in the shape of the Compton profile with increasing Li concentration is consistent with the appearance of states of mainly O $2p$ character. These authors also noted a negative excursion in the so-called "difference Compton profile" (i.e., the difference between the Compton profile of the cathode with higher Li concentration and the cathode with lower Li concentration) as a basis for adducing the presence of signatures of Mn $3d$ electrons becoming more itinerant (less localized) with increasing Li content. The mechanism is that when electrons enter O $2p$ states, they hybridize with the transition metal (TM) $3d$ states and induce delocalization of the Mn $3d$ states. A similar study in Li$_x$CoO$_2$ (LCO) [5] identified the aforementioned negative excursion as a descriptor for improved electrochemical operation in cationic redox reactions. In fact, this descriptor, called the

delocalization profile, was shown to correctly point to the Li concentration range that exhibits improved cathode operation in both LMO and LCO cathodes. In high-capacity Li-excess systems [6], such as Li$_x$Ti$_{0.4}$Mn$_{0.4}$O$_2$ (LTMO), cationic redox reactions are complemented by anionic ones [1]. The anionic redox reaction in LTMO produces a positive tail in the difference Compton profile spectrum at higher momentum, called the *Coulomb profile*, as opposed to the delocalization profile. This behavior implies that electrons introduced into O $2p$ states repel other electrons in the Mn $3d$ states, resulting in the localization of both O $2p$ and Mn $3d$ electrons.

Interestingly, a recent study by Menon *et al.* [7] utilized high-resolution oxygen K-edge resonant inelastic x-ray spectroscopy (RIXS) to investigate LiNi$_{0.98}$W$_{0.02}$O$_2$. This study provided insight into the crucial role of oxygen ions and presented evidence of anionic redox in this non-Li-excess system. This finding is in contrast to a previous x-ray Compton scattering study by Chabaud *et al.* [8] in LiNiO$_2$ (LNO) that suggested cationic redox. These contrasting results have left the question of the nature of hole states in Li-doped NiO controversial.

Here, we address the oxygen character of the redox orbital in LNO and the issues raised by RIXS experiments [9]. In this connection, utilizing high-quality LNO samples [10,11], we performed x-ray Compton scattering measurements along with parallel first-principles modeling of the associated electronic and magnetic structures. Our analysis reveals the coexistence of orbital delocalization produced by Ni-O hybridization and the presence of a dominant O $2p$ character in the redox orbital. Our study suggests that the electronic

---

*veenavee.kothalawala@lut.fi

redistribution in LNO is favorable for Li-ion battery applications and the development of Ni-rich cathode materials for next-generation Li-ion batteries [12].

II. METHODS

A. Samples

Spherical $Ni(OH)_2$ precursors were synthesized using alkali metal hydroxide (NaOH) coprecipitation in an inert gas (nitrogen) atmosphere (see Välikangas *et al.* [10,11] and Zhou *et al.* [13] for details). Inert gas was used to prevent the oxidation of $Ni(OH)_2$ precursor. Precipitation was conducted in a stirred-tank reactor (CSTR) with a reactor volume of 3 L at temperatures of $50\,^\circ C$ under vigorous agitation. Aqueous solutions of metal sulfate $NiSO_4 \cdot 6H_2O$, NaOH, and concentrated ammonia were fed into the reactor using peristaltic pumps. The ammonia concentration in the solution was adjusted based on the target ammonia concentration during the experiment. Particle size growth during $Ni(OH)_2$ coprecipitation was followed by determining the particle size distribution of the slurry sampled from the reactor's overflow tubing. The solution was heated to a precipitation temperature, and the *p*H was adjusted to a desired level with NaOH solution. The feeding rates of nickel sulfate, NaOH, and ammonia solutions were adjusted to maintain the desired residence time. After coprecipitation, the precursor slurry was filtered in a vacuum, and the precipitate was carefully washed with an adequate amount of de-ionized water. The synthesized $Ni(OH)_2$ precursors were dried overnight at $60\,^\circ C$ in a vacuum oven. The material was milled and sieved $40\,\mu m$ in dry room conditions. $Ni(OH)_2$ precursors were mixed with LiOH. Nonstoichiometric Li:Ni mole ratios from zero to one were used. Correspondingly, samples denoted LNO_x were obtained for $x = 0$, $x = 0.25$, $x = 0.5$, $x = 0.75$, and $x = 1$. The mixtures were calcined with a $2.5\,^\circ C/min$ heating ramp and 5 h holding time at a temperature of $670\,^\circ C$ under an O_2 atmosphere. The sample with a lithium concentration of x can be written as $Li_xNi_{2-x}O_2$ as confirmed by the comprehensive sample characterization process discussed in the Supplemental Material (SM) [14]. In particular, the measured x-ray diffraction patterns are in excellent agreement with theoretical predictions by Choi *et al.* [15]. Notably, Välikangas *et al.* (2022) have demonstrated that our fully lithiated samples exhibit high capacity and excellent capacity retention. Also, since we did not cycle the cathode materials in the current Compton study, there is no Li/Ni disordering.

B. Compton profiles

The Compton profile $J(p_z)$ can be calculated within the *impulse approximation* [16,17] using the formula

$$J(p_z) = \iint \rho(\mathbf{p}) dp_x\, dp_y, \tag{1}$$

where $\mathbf{p} = (p_x, p_y, p_z)$ is the electron momentum, and $\rho(\mathbf{p})$ is the electron momentum density that can be expressed as

$$\rho(\mathbf{p}) = \sum_j n_j \left| \int \Psi_j(\mathbf{r}) \exp(-i\mathbf{p}\cdot\mathbf{r}) d^3\mathbf{r} \right|^2. \tag{2}$$

The electron momentum density can be cast in terms of natural orbitals $\Psi_j(r)$, which are the eigenstates of the one-particle density matrix of the many-electron system, and their occupation numbers, n_j [18]. Here, we consider the *independent particle model*, where $n_j = 1$ if the state is occupied and $n_j = 0$ otherwise. The magnetic Compton profile $J_{\mathrm{mag}}(p_z)$ is given by

$$J_{\mathrm{mag}}(p_z) = \iint [\rho_\uparrow(\mathbf{p}) - \rho_\downarrow(\mathbf{p})] dp_x dp_y, \tag{3}$$

where $\rho_\uparrow(\mathbf{p})$ and $\rho_\downarrow(\mathbf{p})$ are the momentum densities of the majority and minority spins, respectively. The spin magnetic moment μ_{spin} is obtained by integrating $J_{\mathrm{mag}}(p_z)$. We then calculate the spherical average of the Compton profile using Monte Carlo sampling coupled with linear interpolation.

Theoretical Compton profiles were computed using density functional theory (DFT) and the tabulated values for the deep core contributions [19]. In DFT, the electron momentum density $\rho(\mathbf{p})$ was obtained from the Kohn-Sham orbitals following Makkonen *et al.* [20] using the Vienna *ab initio* simulation package (VASP) [21,22] and the projector augmented-wave (PAW) method [23]. The generalized gradient approximation (GGA) exchange-correlation functional parametrized by Perdew, Burke, and Ernzerhof (PBE) was used [24] with a kinetic energy cutoff of 520 eV for the plane-wave basis set. To account for electron correlation effects, a Hubbard parameter $U = 4$ eV was applied to Ni $3d$ electrons following earlier studies [25–27]. The Brillouin zone of the supercell was sampled using a uniform Γ-centered $4 \times 8 \times 4$ k-point grid.

Compton and magnetic Compton profiles were measured at the high-energy inelastic scattering beamline 08W at the Japanese synchrotron facility SPring-8 [28,29]. Circularly polarized x rays of 182.6 keV emitted from an elliptical multipole wiggler were irradiated to the sample. The size of the incident x-ray beam at the sample position is a 1 mm square. Compton scattered x rays were measured using a pure Ge solid-state detector. The scattering angle was fixed at 178°, and Compton profiles were measured at room temperature. For magnetic Compton profiles, a magnetic field of ±2.5 T was applied to the sample that was kept at 7 K to obtain Compton scattered x-ray intensities, I_+ and I_-, by flipping the magnetic field every 60 s.

III. RESULTS AND DISCUSSION

We begin by examining the Compton profiles of Li-doped NiO (Fig. 1). Theoretical profiles for both LNO and NiO agree well with the corresponding experimental results, indicating that the Kohn-Sham orbitals employed in our DFT calculations accurately capture the electron momentum distribution in Li-doped Ni oxide.

We isolate the signature of the redox orbital by subtracting the NiO_2 contribution from the valence Compton profile of $LiNiO_2$. The result is given by

$$\Delta J(p) = J_v^{\mathrm{LiNiO_2}}(p) - J_v^{\mathrm{NiO_2}}(p), \tag{4}$$

where $J_v^{\mathrm{LiNiO_2}}(p)$ is the spherical average valence Compton profile for LNO while $J_v^{\mathrm{NiO_2}}(p)$ is the spherical average valence Compton profile for NiO_2. Since the experimental
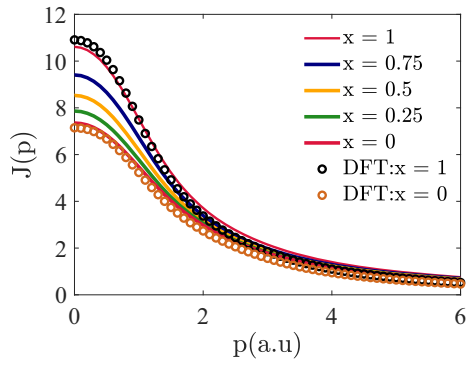
FIG. 1. Experimental and theoretical total Compton profiles (spherical averaged) for various x values. Theoretical profiles are convoluted with a Gaussian of 0.5 a.u. full width at half maximum. All profiles are normalized to the electrons per nickel atom (i.e., $Li_{x/(2-x)}NiO_{2/(2-x)}$).

Compton profile of NiO_2 is not available, this analysis only involves our first-principles results (Fig. 2). As discussed previously [1,5], the difference profile can be rationalized using a model with Slater orbitals, which involves two main contributions: the atomic O-$2p$ Compton profile and the so-called delocalization profile. To model these contributions, we utilize the radial wave functions given by Slater orbitals, characterized by effective exponents Z_{eff} that are fitted to the DFT profile (see SM [14] for details). The importance of the O $2p$ character has been previously observed in connection with XAS experiments [30], while the existence of the delocalization profile $D(p)$ is necessary to explain the negative excursion in the difference Compton profile. The delocalization profile
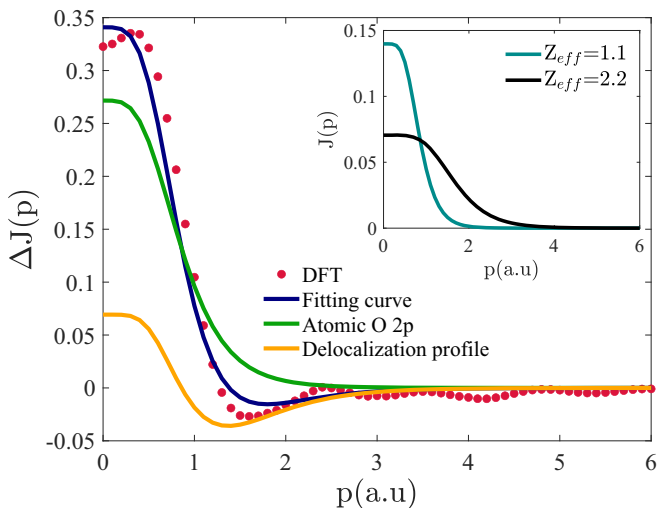

FIG. 2. Theoretical difference valence Compton profiles (spherical averaged) of LNO and NiO_2, along with the corresponding curve-fitting results (solid lines). Contributions of O $2p$ and Ni $3d$ electrons are included. The inset provides Compton profiles of Ni $3d$ orbital states for two different values of Z_{eff}. The Delocalization profile is determined by the difference between the profile for $Z_{eff} = 2.2$ and the profile for $Z_{eff} = 1.1$. The area under the negative excursion of the profiles gives the number of electrons delocalizing in the lithiation process.
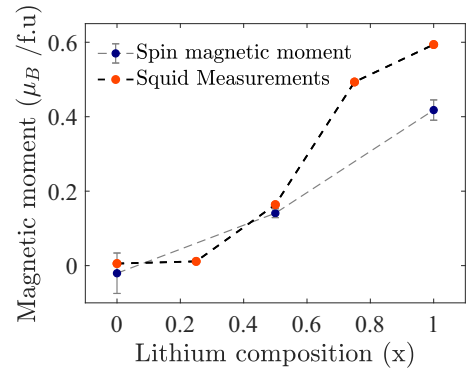

FIG. 3. Spin magnetic moments for various Li concentrations x. The dashed line is a guide to the eye.

also allows us to quantify the number of electrons delocalizing in the lithiation process in terms of the integral $\int dp |D(p)|$. We estimate this number to be 0.089 electrons per Li atom.

With the preceding results in mind, we are in a position to provide a clearer explanation of the significant physics revealed by our study regarding LNO. Our VASP first-principles calculations clearly show that the number of electrons in the interstitial region increases with increasing lithium concentration while the number of electrons on the nickel sites remains constant, as also shown by Genreith-Schriever and collaborators [31]. A similar behavior was observed by Suzuki *et al.* [4] in LMO. The number of electrons within the oxygen muffin-tin spheres also remains constant, although some of the additional charge in the interstitial region belongs to the oxygen atoms. These results strongly suggest a significant delocalization of oxygen $2p$ character and a dominant involvement of oxygen in the redox process. This process also leads to a redistribution of Ni $3d$ electrons and results in a favorable orbital delocalization that supports battery operation.

Goodenough and colleagues first observed the ferromagnetic nature of LNO in 1958 [32]. This intriguing ferromagnetic phase has since been confirmed by accurate diffusion quantum Monte Carlo (DQMC) calculations [33] and further discussed in a recent review by Tranquada [34]. Leveraging ferromagnetism, we conducted magnetic Compton scattering experiments on LNO samples with varying Li concentrations (x). Figure 3 shows magnetic moments as a function of x so obtained along with the values we obtained using superconducting quantum interference device (SQUID) measurements. Although the SQUID values exceed the values obtained via magnetic Compton scattering, both sets consistently yield an increasing magnetic moment with x. The discrepancy between the two measurements arises from the fact that SQUID measures the total moment (i.e., orbital and spin moment), while magnetic Compton scattering only provides the spin moment.

Notably, the magnetic moment in our case did not reach saturation under the field of 2.5 T, which was used in both the magnetic Compton scattering and SQUID experiments. This lack of saturation is a significant factor contributing to the discrepancy between our measurement and our theoretical predictions, which give a magnetic moment of $1\mu_B$ for $x = 1$.

Magnetic Compton profiles for $x = 1$ and $x = 0.5$ exhibit a remarkable similarity in that the two profiles can be
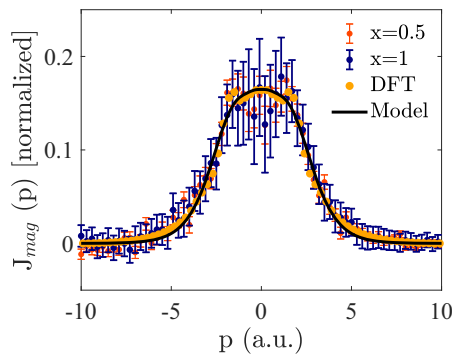
FIG. 4. Magnetic Compton profiles (spherical averaged) for $x = 1$, and $x = 0.5$. The DFT calculation is for $x = 1$.

FIG. 5. Spin density in LNO using an isosurface value of 0.01 a.u. on Li (green), Ni (gray), and O (red).

collapsed onto a single curve when normalized to the same scale (Fig. 4). It is important to distinguish between the difference Compton profile and the magnetic Compton profiles, as they offer complementary insights into the redox and magnetic orbitals, respectively [35]. To capture the shape of the magnetic Compton profile, we employed a fitted model using a Ni $3d$ Slater orbital with $Z_{eff} = 3.8$. Additionally, we included a small magnetic contribution from O $2p$ orbitals with $Z_{eff} = 1.1$, reflecting the mixing of a few percent due to the presence of a small local magnetic moment on the oxygen site. This fitted model is consistent with the LNO spin density calculated within the DFT, as shown in Fig. 5. Interestingly, our findings indicate a positive magnetization on the O atom, while the DQMC [33] predicts a negative contribution because of the approximate $R\bar{3}m$ crystal symmetry used in the DQMC calculation.

IV. CONCLUSION

We utilize x-ray Compton scattering along with parallel first-principles modeling to investigate the electronic structure of LNO cathode materials to gain insight into the delithiation process of going from $LiNiO_2$ to NiO_2. By directly measuring the electron density distribution (spherically averaged) of individual orbitals in momentum space, we showcase the unique ability of the Compton scattering technique to extract redox and magnetic orbit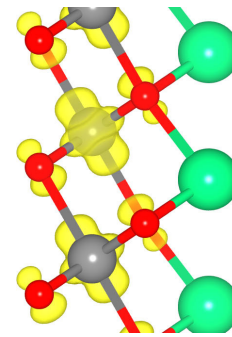als realistically. Our analysis reveals that the Ni charge in NiO, NiO_2, and $LiNiO_2$ is the same, while the occupation of oxygen orbitals changes with lithiation, indicating that O dominates the underlying charge-transfer mechanism. These results help explain oxygen loss in Ni-rich layered cathode materials, reported in recent RIXS experiments [7]. Our study also sheds light on the role of $3d$ electron delocalization in the layered LNO chemistry, highlighting its importance in the redox processes.

[1] H. Hafiz, K. Suzuki, B. Barbiellini, N. Tsuji, N. Yabuuchi, K. Yamamoto, Y. Orikasa, Y. Uchimoto, Y. Sakurai, H. Sakurai, A. Bansil, and V. Viswanathan, Tomographic reconstruction of oxygen orbitals in lithium-rich battery materials, Nature (London) **594**, 213 (2021).

[2] J. Nokelainen, B. Barbiellini, J. Kuriplach, S. Eijt, R. Ferragut, X. Li, V. Kothalawala, K. Suzuki, H. Sakurai, H. Hafiz, K. Pussi, F. Keshavarz, and A. Bansil, Identifying redox orbitals and defects in lithium-ion cathodes with compton scattering and positron annihilation spectroscopies: A review, Condensed Matter **7**, 47 (2022).

[3] G. Pagot, V. Di Noto, K. Vezzù, B. Barbiellini, V. Toso, A. Caruso, M. Zheng, X. Li, and R. Ferragut, Quantum view of Li-ion high mobility at carbon-coated cathode interfaces, iScience **26**, 105794 (2023).

[4] K. Suzuki, B. Barbiellini, Y. Orikasa, N. Go, H. Sakurai, S. Kaprzyk, M. Itou, K. Yamamoto, Y. Uchimoto, Y. J. Wang, H. Hafiz, A. Bansil, and Y. Sakurai, Extracting the redox orbitals in Li battery materials with high-resolution x-ray Compton scattering spectroscopy, Phys. Rev. Lett. **114**, 087401 (2015).

[5] B. Barbiellini, K. Suzuki, Y. Orikasa, S. Kaprzyk, M. Itou, K. Yamamoto, Y. J. Wang, H. Hafiz, R. Yamada, Y. Uchimoto, A. Bansil, Y. Sakurai, and H. Sakurai, Identifying a descriptor for d-orbital delocalization in cathodes of Li batteries based on x-ray Compton scattering, Appl. Phys. Lett. **109**, 073102 (2016).

[6] G. Assat and J.-M. Tarascon, Fundamental understanding and practical challenges of anionic redox activity in Li-ion batteries, Nat. Energy **3**, 373 (2018).

[7] A. S. Menon, B. Johnston, S. G. Booth, L. Zhang, K. Kress, B. Murdock, G. Fajardo, N. N. Anthonisamy, N. T. Ruiz,

S. Agrestini, K. Zhou, T. Lee, A. Nedoma, S. Cussen, and L. Piper, Oxygen-redox activity in non-Li-excess W-doped $LiNiO_2$ cathode, ChemRxiv (2022).

[8] S. Chabaud, C. Bellin, F. Mauri, G. Loupias, S. Rabii, L. Croguennec, C. Pouillerie, C. Delmas, and T. Buslaps, Electronic density distortion of NiO_2 due to intercalation by Li, J. Phys. Chem. Solids **65**, 241 (2004).

[9] N. Li, S. Sallis, J. K. Papp, J. Wei, B. D. McCloskey, W. Yang, and W. Tong, Unraveling the cationic and anionic redox reactions in a conventional layered oxide cathode, ACS Energy Lett. **4**, 2836 (2019).

[10] J. Välikangas, P. Laine, M. Hietaniemi, T. Hu, P. Tynjälä, and U. Lassi, Precipitation and calcination of high-capacity $LiNiO_2$ cathode material for lithium-ion batteries, Appl. Sci. **10**, 8988 (2020).

[11] J. Valikangas, P. Laine, M. Hietaniemi, T. Hu, M. Selent, P. Tynjälä, and U. Lassi, Correlation of aluminum doping and lithiation temperature with electrochemical performance of LiNiO cathode material, J. Solid State Electrochem. **27**, 641 (2022).

[12] M. Bianchini, M. Roca-Ayats, P. Hartmann, T. Brezesinski, and J. Janek, There and back again—the journey of $LiNiO_2$ as a cathode active material, Angew. Chem., Int. Ed. **58**, 10434 (2019).

[13] F. Zhou, X. Zhao, van A. Bommel, A. Rowe, and J. R. Dahn, Coprecipitation synthesis of $Ni_xMn_{1-x}(OH)_2$ mixed hydroxides, Chem. Mater. **22**, 1015 (2010).

[14] See Supplemental Material at http://link.aps.org/supplemental/10.1103/PhysRevB.109.035139 for the characterization of the samples and about the DFT calculations (DOS), which includes Refs. [36–39].

[15] D. Choi, J. Kang, and B. Han, Unexpectedly high energy density of a Li-ion battery by oxygen redox in $LiNiO_2$ cathode: First-principles study, Electrochim. Acta **294**, 166 (2019).

[16] I. G. Kaplan, B. Barbiellini, and A. Bansil, Compton scattering beyond the impulse approximation, Phys. Rev. B **68**, 235104 (2003).

[17] M. Cooper, P. Mijnarends, N. Shiorani, N. Sakai, and A. Bansil, in *X-Ray Compton Scattering* (Oxford University Press, Oxford, UK, 2004), pp. 31–39.

[18] B. Barbiellini and A. Bansil, Treatment of correlation effects in electron momentum density: Density functional theory and beyond, J. Phys. Chem. Solids **62**, 2181 (2001).

[19] F. Biggs, L. Mendelsohn, and J. Mann, Hartree-Fock Compton profiles for the elements, At. Data Nucl. Data Tables **16**, 201 (1975).

[20] I. Makkonen, M. Hakala, and M. Puska, Calculation of valence electron momentum densities using the projector augmented-wave method, J. Phys. Chem. Solids **66**, 1128 (2005).

[21] G. Kresse and J. Furthmüller, Efficiency of ab-initio total energy calculations for metals and semiconductors using a plane-wave basis set, Comput. Mater. Sci. **6**, 15 (1996).

[22] G. Kresse and D. Joubert, From ultrasoft pseudopotentials to the projector augmented-wave method, Phys. Rev. B **59**, 1758 (1999).

[23] P. E. Blöchl, Projector augmented-wave method, Phys. Rev. B **50**, 17953 (1994).

[24] J. P. Perdew, K. Burke, and M. Ernzerhof, Generalized gradient approximation made simple, Phys. Rev. Lett. **77**, 3865 (1996).

[25] M. Tuccillo, O. Palumbo, M. Pavone, A. Muñoz-García, A. Paolone, and S. Brutti, Analysis of the phase stability of $LiMO_2$ layered oxides (M = Co, Mn, Ni), Crystals **10**, 526 (2000).

[26] L. Wang, T. Maxisch, and G. Ceder, Oxidation energies of transition metal oxides within the GGA + U framework, Phys. Rev. B **73**, 195107 (2006).

[27] V. N. Kothalawala, A. A. S. Devi, J. Nokelainen, M. Alatalo, B. Barbiellini, T. Hu, U. Lassi, K. Suzuki, H. Sakurai, and A. Bansil, First principles calculations of the optical response of $LiNiO_2$, Condens. Matter **7**, 54 (2022).

[28] Y. Sakurai, High-energy inelastic-scattering beamline for electron momentum density study, J. Synchrotron Radiat. **5**, 208 (1998).

[29] Y. Kakutani, Y. Kubo, A. Koizumi, N. Sakai, B. L. Ahuja, and B. K. Sharma, Magnetic Compton profiles of fcc-Ni, $fcc-Fe_{50}Ni_{50}$ and hcp-Co, J. Phys. Soc. Jpn. **72**, 599 (2003).

[30] P. Kuiper, G. Kruizinga, J. Ghijsen, G. A. Sawatzky, and H. Verweij, Character of holes in $Li_xNi_{1-x}O$ and their magnetic behavior, Phys. Rev. Lett. **62**, 221 (1989).

[31] A. R. Genreith-Schriever, H. Banerjee, A. S. Menon, E. N. Bassey, L. F. Piper, C. P. Grey, and A. J. Morris, Oxygen hole formation controls stability in $LiNiO_2$ cathodes, Joule **7**, 1623 (2023).

[32] J. B. Goodenough, D. G. Wickham, and W. J. Croft, Some ferrimagnetic properties of the system $Li_xNi_{1-x}O$, J. Appl. Phys. **29**, 382 (1958).

[33] K. Saritas, E. R. Fadel, B. Kozinsky, and J. C. Grossman, Charge density and redox potential of $LiNiO_2$ using *ab initio* diffusion quantum Monte Carlo, J. Phys. Chem. C **124**, 5893 (2020).

[34] J. M. Tranquada, John Goodenough and the many lives of transition-metal oxides, J. Electrochem. Soc. **169**, 010535 (2022).

[35] K. Suzuki, Y. O. K. Hoshi, H. Sakurai, N. Tsuji, K. Yamamoto, N. Yabuuchi, H. Hafiz, Y. Orikasa, Y. Uchimoto, Y. Sakurai, V. Viswanathan, A. Bansil, and B. Barbiellini, Magnetic compton scattering study of Li-rich battery materials, Condens. Matter **7**, 4 (2022).

[36] FE-SEM, Carl Zeiss Microscopy GmbH, Germany.

[37] A Rigaku SmartLab.

[38] Thermo Electron iCAP 6500 Duo, Thermo Fisher Scientific, USA.

[39] Quantum Design Japan, Inc.